The Secondary Structure of the Inhibited Mitochondrial ADP/ATP Transporter from Yeast Analyzed by FTIR Spectroscopy[†]

Víctor A. Lórenz,[‡] Joaquim Villaverde,[‡] Véronique Trézéguet,[§] Guy J.-M. Lauquin,[§] Gérard Brandolin,[||] and Esteve Padrós*,[‡]

Unitat de Biofisica, Departament de Bioquímica i de Biologia Molecular, Facultat de Medicina, Universitat Autònoma de Barcelona, 08193 Bellaterra, Barcelona, Spain, Laboratoire de Physiologie Moléculaire et Cellulaire, Institut de Biochimie Cellulaire du CNRS, 1 rue Camille Saint Saëns, 33077 Bordeaux Cedex, France, and Laboratoire de Biochimie et Biophysique des Systèmes Intégrés, UMR 5092 CEA-CNRS-UJF, Département de Biologie Moléculaire et Structurale, CEA/Grenoble, 17 rue des Martyrs, 38054 Grenoble Cedex 9, France

Received January 16, 2001; Revised Manuscript Received April 10, 2001

ABSTRACT: Fourier transform infrared spectroscopy has been applied to the study of the carboxyatractyloside-inhibited mitochondrial ADP/ATP transporter from the yeast *Saccharomyces cerevisiae*, either solubilized in dodecyl maltoside or reconstituted in phosphatidylcholine liposomes. Its secondary structure has been estimated by means of Fourier self-deconvolution followed by curve fit. A Voigt function was used to fit the components of the deconvoluted spectrum, aiming to account for any distortions introduced by deconvolution. For any of the states analyzed, reconstituted or solubilized, in solution or in dry films, 60−70% of the amino acids are found to adopt α-helix plus unordered structures, coherent with the six transmembrane spanning helix model. Moreover, the problem of structure preservation on drying was addressed, and several observations pointed to a maintenance of the protein structure in dry films. Comparison of reconstituted and solubilized samples indicated the presence of both lipid-induced changes in the protein (decrease of the β-sheets and increase of unordered structures) and protein-induced changes in the lipids (strong hydrogen bonding of lipid C═O groups). To obtain a better discrimination of α-helix and unordered structure contributions for the reconstituted form, H/D exchange experiments were performed. Between 35% and 45% of the amino acids were finally assigned to α-helix structures, compatible with the existence of five or six transmembrane spanning helices in the transporter. The level of H/D exchange was determined after 15 h of exposure to D_2O vapor to be 85%, reflecting a high accessibility of the amide hydrogens even for the carboxyatractyloside-inhibited state.

The ADP/ATP carrier is a protein of the inner mitochondrial membrane, which exclusively catalyzes the 1-to-1 exchange of cytosolic ADP, imported into mitochondria, for ATP generated in the matrix space by oxidative phosphorylation. The ADP/ATP transport system can be blocked by very specific inhibitors, which bind to the carrier with high affinity. They belong to two families: atractyloside and carboxyatractyloside on one hand, which bind to the transporter in the so-called CATR conformation, and bongkrekic acid and isobongkrekic acid on the other hand, able to bind to the transporter in the so-called BA conformation. Binding of the inhibitors to the carrier results in carboxyatractyloside− and bongkrekic acid−carrier complexes, which exhibit different chemical, immunochemical, and enzymatic reactivities. It has been suggested that the transition between the CATR and BA conformations is involved in the ADP/ATP transport process (for a review see ref *1*). Therefore, structural analysis of these complexes would be invaluable in understanding the nucleotide transport mechanism at the molecular level.

In the yeast *Saccharomyces cerevisiae*, three highly similar genes encoding the ADP/ATP carrier have been isolated (*2*−*4*). Only the ANC2 isoform is required for the cells to grow on a nonfermentable carbon source, such as glycerol or lactate (*5*, *6*). In this study we used the yeast mitochondrial ADP/ATP carrier isolated from a genetically modified strain of *S. cerevisiae*, which produces the His-tagged Anc2p[1] isoform of the carrier (Anc2pHis).

Infrared spectroscopy, through the study of the protein amide I and amide II bands, has been proven to be a valuable tool for the protein secondary structure estimation (*7*−*9*).

[†] This work was supported by Grants Bio4-CT97-2119 from the European Commission (to G.B., G.J.-M.L., and E.P.) and 1999SGR00102 from the Direcció General de Recerca (Generalitat de Catalunya) and Fellowship 1998-FI-00215 from the DGR (Generalitat de Catalunya) (to V.A.L.). J.V. is a fellow of the European Commission (Bio4-CT97-2119).

* Corresponding author. Tel: +34-935811870. Fax: +34-935811907. E-mail: esteve.padros@uab.es.

[‡] Universitat Autònoma de Barcelona.

[§] Institut de Biochimie Cellulaire du CNRS.

[||] CEA/Grenoble.

[1] Abbreviations: Anc2p, mitochondrial ADP/ATP transporter; Anc2pHis, 6 histidine tagged mitochondrial ADP/ATP transporter; ATR, attenuated total reflection; DM, dodecyl maltoside; FTIR, Fourier transform infrared; FWHH, full width at half-height; FSD, Fourier self-deconvolution; IR, infrared; *k*, narrowing factor; n_1, n_2, and n_3, refractive index of the ATR crystal, sample, and air; γ, FWHH of a band before FSD; γ', FWHH used in FSD; ϵ, absorption coefficient; *B*, integrated absorption coefficient; *p*, order parameter of the dipole transition moment; E_x, E_y, and E_z, time averaged electric fields; θ, angle between the IR beam and the crystal surface normal; egg PC/PA, egg phosphatidylcholine and phosphatidic acid; S/N, signal-to-noise standard deviation ratio.

10.1021/bi010091s CCC: $20.00
Published on Web 06/30/2001

The correlation between amide I and amide II band position and secondary structure has been demonstrated from both experimental studies on homopeptides of known secondary structures (*10*, *11*) and theoretical studies on homopeptides with pure secondary structure (*10*, *12*). Spectra deconvolution followed by curve fitting has been used to resolve the contributions of the different secondary structures in the amide I (*13*, *14*). Gaussian, Lorentzian, and mixed Gaussian−Lorentzian bands have been used to fit deconvoluted spectra, although without a clear justification. In the present work Voigt functions have been used to curve fit deconvoluted spectra. When this band profile is used, reliable estimates for position, width, and area of the components bands are obtained, increasing the reliability of the final fit to this spectrum (results to be published).

Infrared spectroscopy also provides the opportunity to study the H/D exchange by following the decrease in the amide II band area. Upon exchange of the hydrogen of the amide groups by deuterium, the amide II band disappears, being reconverted in two new bands; one of them, called amide II′, appears 100 cm^{-1} down from the amide II, and the second one appears around 1000 cm^{-1} (*8*, *9*). Although major information comes from the analysis of the kinetics of exchange (*15*), the total exchange at an appropriated long time of exchange can give some clues to the accessibility of the amide hydrogen atoms to the solvent and provides a way to compare the Anc2p with other membrane proteins.

These spectroscopic techniques were used in the present work to get an approach to the secondary structure of the adenine nucleotide carrier Anc2p from yeast. Unfortunately, the free form of the Anc2p has been shown to be very labile when isolated from mitochondria (*16*). After an exhaustive purification at least half of the binding sites are commonly lost (*17*, *18*). Attempts have been done to shorten the time the protein spends solubilized in detergent, aiming to reduce lose of protein binding sites. Regrettably, after this fast purification procedure the protein purity decreased dramatically to half of the total protein (*19*). As a consequence the present studies were restricted to the carboxyatractyloside-inhibited transporter in order to have pure protein blocked in a well-defined conformational state. It is important to realize that carboxyatractyloside binds tightly to the protein in one of the conformations involved in the ATP/ADP transport (the CATR conformation), and although not active, the resultant complex should display a structure very similar to that of the free protein in the CATR conformation and thus should be considered as a good model for this conformation. As a conclusion, the presence of the inhibitor, although avoiding the achievement of any functional studies, should not affect structural studies to be done.

Two forms of inhibited Anc2pHis sample preparations were used, solubilized in the nondenaturing detergent dodecyl maltoside or reconstituted in negatively charged liposomes, to test the influence of the hydrophobic environment surrounding the carrier, either micellar or membrane bilayer, respectively. Moreover, the suitability of studying the Anc2pHis preparations in the form of dry films was tested.

MATERIALS AND METHODS

Yeast Strains and Media. We used the genetically modified JL1-3-ANC2(His6) *S. cerevisiae* yeast strain, which produced a modified isoform of Anc2p containing the extra sequence GSRSHHHHHH at its C-terminal end (Anc2pHis) (*20*). JL1-3-ANC2(His6) yeast cells were grown as described (*17*).

Preparation of Yeast Mitochondria. Yeast cells were harvested during exponential growth phase when the OD 540 nm reached a value of 5.0. Mitochondria were prepared as described (*21*). Briefly, protoplasts obtained by enzymatic digestion of the cell wall with Zymolyase 20T (Seikagaku Corp.) were disrupted with a Dounce homogenizer in a medium made of 0.6 M mannitol, 0.1 mM EDTA, 10 mM Tris-HCl, 0.1% BSA. and 1 mM phenylmethanesulfonyl fluoride (PMSF), pH 7.4. Mitochondria were isolated by differential centrifugation, washed with the same medium but devoid of BSA and PMSF, and stored in liquid nitrogen.

Purification of the Carboxyatractyloside-Inhibited Anc2pHis. All purification steps were carried out at 4 °C. Isolated yeast mitochondria were preincubated with carboxyatractyloside, suspended at 10 mg of protein/mL in 0.1 M Na_2SO_4, 1 mM EDTA, 1 mM diisopropyl fluorophosphate, and 10 mM Tris-HCl, pH 7.3, and solubilized by addition of 1% DM and 1% Emulphogen BC720. The soluble extract was submitted to hydroxylapatite (HTP) chromatography (*22*) with modifications (*17*). Partially purified Anc2p and Anc2pHis were recovered in the flow-through fraction. Anc2pHis was further purified by immobilized metal ion affinity chromatography (IMAC) using the Ni−NTA resin, following the experimental conditions previously established (*20*). Briefly, Anc2pHis was bound to the resin in the presence of 5 mM $MgSO_4$, 50 mM NaP_i, pH 7.3, and 0.1% DM. After extensive washing of the resin, it was eluted by 500 mM imidazole in 50 mM NaCl and 10 mM Mes, pH 6.8, with 0.02% DM. Pure Anc2pHis was then subjected to a overnight dialysis at 4 °C in front of 50 mM NaCl and 10 mM Mes, pH 6.8, with 0.015% DM. In these conditions the carboxyatractyloside-inhibited Anc2pHis was obtained at a concentration of about 0.04 mg/mL. The presence and purity of protein from the HTP chromatography and the Ni−NTA batch eluates were determined from a 12% SDS−PAGE stained with Coomassie Blue (see Figure 1). For IR studies, solubilized Anc2pHis was concentrated using Centriprep YM30 (Amicon). Final concentration was measured by UV−vis absorbance at 280 nm using ϵ_{280}(Anc2p) = 0.9 $(g/mL)^{-1}$ cm^{-1} [from ϵ_{280}(Trp) = 4500 M^{-1} cm^{-1} and ϵ_{280}(Tyr) = 1500 M^{-1} cm^{-1}], and by the bicinchoninic acid method (*23*), giving similar results.

Reconstitution of the Carboxyatractyloside-Inhibited Anc2pHis. To the purified Anc2pHis was added egg PC/PA (1:1 w/w) presolubilized with DM to a final lipid-to-protein ratio of 3:1 (w/w) and final DM-to-lipid ratio of 2:1 (w/w). After 1−2 h of incubation at 4 °C, Bio-Beads were added to a final ratio to DM of 33:1 (w/w). After 6 h of soft stirring at 4 °C the proteoliposomes obtained were centrifuged at 90000*g* for 90 min. The pellet was resuspended to the final concentration used in the experiments.

FTIR Transmission Experiments. (A) Sample Preparation. For IR transmission experiments of solubilized samples in solution, the carboxyatractyloside-inhibited Anc2pHis was dissolved at a concentration of 10 mg/mL, in 9.2% DM, 10 mM Mes, and 50 mM NaCl (pH 6.8), and was placed between two CaF_2 windows using a 6 μm tin spacer. For transmission spectra of dry fims of solubilized protein, 0.2

mg of protein was spread over a CaF_2 window and dried under vacuum.

(B) Spectra Acquisition. A total of 1000 scans were coadded in blocks of 40 reference scans and 40 sample scans using a shuttle accessory, with an instrumental resolution of 2 cm^{-1} on a Mattson Polaris FTIR equipped with an MCT detector. The resulting interferogram was apodized with a triangle function and processed to give an absorption spectra at 0.5 cm^{-1} digital resolution. The sample was placed in a circulating water holder connected to a thermostatic bath. An external probe fitted to the sample holder was used to keep the temperature at 25.0 ± 0.05 °C. The spectrometer compartment was purged with dry air, having finally a dew point lower than −50 °C. This low water vapor concentration, together with the spectra acquisition in blocks, usually gave absorption spectra free from water vapor bands.

(C) Buffer Subtraction. For transmission experiments in solution a buffer spectrum was collected and subtracted to eliminate the contribution of water, detergent, and salts. The subtraction factor was chosen as that leaving a flat baseline between 2000 and 1800 cm^{-1}.

FTIR Attenuated Total Reflection Experiments. (A) Sample Preparation. Eighty micrograms of the carboxyatractyloside-inhibited protein at a concentration of 4 mg/mL, in 12 mg/mL egg PC/PA (1:1 w/w), 10 mM Mes, and 50 mM NaCl (pH 6.8), was spread on a 45° trapezoid ATR germanium crystal of 50 × 20 × 10 mm. The sample was dried at the atmospheric humidity first and under a dry nitrogen flow later.

(B) Exchange Experiments. A dry film of the reconstituted protein was exposed to a continuous flow of dry nitrogen (150 mL/min) saturated of D_2O at 26 °C. The amide I area was measured from 1690 to 1615 cm^{-1}. For the amide II two intervals were used, 1580−1520 cm^{-1} and 1560−1530 cm^{-1}. When the broader interval was used, a slightly higher exchange level was measured.

(C) Spectra Acquisition. A total of 2000 scans were coadded at an instrumental resolution of 2 cm^{-1} on a Bio-Rad FTS 6000 spectrometer equipped with an MCT detector. The resulting interferogram was apodized with a triangle function and processed to give an absorption spectrum at 0.5 cm^{-1} digital resolution. A cover jacket was placed over the ATR crystal and connected to a circulating thermostatic bath at 26 °C. The spectrometer compartment was purged with dry air, having finally a dew point lower than −40 °C. No block averaging was used; under these conditions the presence of residual water vapor peaks in the absorption spectra cannot be fully prevented, so water vapor was collected and subtracted when needed.

(D) Characterization of the Films Used in ATR-FTIR. It is necessary to determine if the films studied by ATR are described by the thin film hypothesis (film thickness infinitesimally small compared to the IR light penetration depth) or by the thick film hypothesis (thickness much bigger that the penetration depth). In the thin film case the effective path length, and therefore the measured absorbance, is proportional to the film thickness, resembling the transmittance spectra. In contrast, in the thick film case the effective path length is independent of the actual film thickness but decreases as the wavenumber increases. Then, comparison between the area ratios of two separated bands obtained from both transmittance and ATR allows the discrimination between thick and thin film hypotheses. For a thin film the area ratio of two bands A_1/A_2 is the same as in transmittance, but for a thick film it becomes $(A_1/A_2)_{trans} = (\nu_1/\nu_2)(A_1/A_2)_{ATR}$, where ν_1 and ν_2 are the positions of the two bands (*15*).

Spectral Corrections and Determination of Experimental Errors. (A) Amino Acid Side Chain Absorption Subtraction. A synthetic amino acid side chain absorption spectrum was constructed from the data of Venyaminov and Kalnin (*24*) for H_2O spectra and Chirgadze et al. (*25*) for D_2O spectra, taking into account the primary sequence of the Anc2pHis (*18*). The subtraction factor was calculated from the protein concentration and path length.

(B) Phospholipid and DM Absorption. The phospholipids used have no significant absorption in the amide I or II, neither between 4000 and 3150 cm^{-1}, so amide A (with maximum around 3290 cm^{-1}) and remaining water (maximum around 3400 cm^{-1}) are directly observed in reconstituted samples. DM shows no absorption in the amide I or II, but it does between 3500 and 3100 cm^{-1}, preventing the direct observation of amide A and remaining water in DM solubilized samples.

(C) Determination of Absorption Coefficients (ϵ) and Integrated Absorption Coefficients (B) by Transmittance. For H_2O solutions, the path length was calculated essentially as described (*26*). However, due to the baseline uncertainty when using MCT detectors (*27*) the difference absorption coefficients between 2125 and 1880 cm^{-1} for H_2O at 25 °C was preferred: $(\epsilon_{2125} - \epsilon_{1880}) = 1.55\ M^{-1}\ cm^{-1}$. Water concentration was calculated assuming a volumetric mass for solutes equal to 1 g/L. For dry films it was assumed that the integrated absorption coefficients for acyl bands of DM and egg PC (3100−2800 cm^{-1}) are independent of the humidity. The following coefficients were determined: DM acyl stretching, $B_{3000-2800} = (187 \pm 14) \times 10^3\ g^{-1}\ cm$; egg PC acyl stretching, $B_{2975-2775} = (212 \pm 14) \times 10^3\ g^{-1}\ cm$; egg PC C═O stretching, $B_{1760-1700} = (18.0 \pm 1.6) \times 10^3\ mmol^{-1}\ cm^{-2}$; and dry film egg PC C═O stretching, $B_{1760-1700} = (22 \pm 4) \times 10^3\ mmol^{-1}\ cm^{-2}$.

(D) Determination of the Signal-to-Noise Ratio. Using an interval free of sample bands (usually between 1800 and 1850 cm^{-1}) a straight line was fitted. The standard deviation of the residual was taken as the noise standard deviation at 1825 cm^{-1} (SD_1). The noise standard deviation at the amide I maximum (SD_2) was calculated as described (*28*) using

$$SD_2 = SD_1 \times 10^{Abs_2 - Abs_1}$$

where Abs_2 is the absorption in the original nonsubtracted spectrum at the amide I maximum and Abs_1 the absorption at 1825 cm^{-1}. Then the signal-to-noise ratio was calculated, taking as signal the absorbance at amide I maximum and as noise the calculated value of SD_2.

(E) Determination of the Error Due to Orientation of the Sample. For a globally oriented protein with axial symmetry relative to the ATR crystal, or to the windows in transmittance setup, even using unpolarized light the absorbance depends on the orientation, leading to errors in quantitative analysis and thus in the estimation of secondary structure of proteins (*29*). The absorbance using unpolarized light is for most interferometers approximately equal to the addition of

the absorbance using parallel and perpendicular polarized light (*15*) according to

$$\mathrm{Abs}_{\mathrm{unpol}} = 0.5\mathrm{Abs}_{90} + 0.5\mathrm{Abs}_{0}$$

We define the relative error of the absorbance of one band corresponding to a globally oriented protein with respect to the same protein with nonglobal orientation as

$$\text{error} = \frac{\mathrm{Abs}_{90}(p) + \mathrm{Abs}_{0}(p)}{\mathrm{Abs}_{90}(p=0) + \mathrm{Abs}_{0}(p=0)} - 1$$

where p is the order parameter of the transition dipole moment of the considered band with respect the surface normal (p is equal to 0 for a nonoriented protein). For ATR, the absorbance depends on optical parameters (see ref *15* for expressions of E_x, E_y, E_z dependency on n_1, n_2, n_3, and θ), and the relative error becomes

$$\text{error} = \frac{(1-p)(E_x^2 + E_y^2) + (2p+1)E_z^2}{E_x^2 + E_y^2 + E_z^2} - 1$$

Taking the thin film hypothesis and using the values for a proteolipid film on a germanium plate ($n_1 = 4.0$, $n_2 = 1.5$, $n_3 = 1.0$, and $\theta = 45°$), the relative error becomes er $= -0.705p$ and goes from -70.5% for $p = 1$ (reduction of absorbance in globally oriented proteins for bands with the transition dipole moment parallel to the crystal surface normal) to $+35\%$ for $p = -0.5$ (enhancement in perpendicular orientation). For the thick film hypothesis in the same conditions the relative error becomes er $= 0.164p$, and it goes from $+16\%$ for $p = 1$ to -8% for $p = -0.5$.

For transmission spectra the relative error is expressed as

$$\text{error} = \frac{2\cos^2\theta(1-p) + \sin^2\theta(2p+1)}{2\cos^2\theta + \sin^2\theta} - 1$$

where θ stands for the angle between the beam and the window normal. In the standard disposition $\theta = 0°$, and the error becomes er $= 1 - p$, going from -100% for $p = 1$ (no band absorption) to $+50\%$ for p $= -0.5$ (absorption enhancement).

Quantitative Analysis of the Spectral Components of Protein Amide I. (A) Fourier Self-Deconvolution and Maximum Likelihood Restoration. These procedures were performed using the programs supplied by Spectrum Square Associates, Inc., implemented in the GRAMS software (Galactic Industries). For Fourier self-deconvolution (referred to in the following as deconvolution) a Lorentzian profile was used, with full width at half-height (FWHH) of γ', filtered with a Bessel function and a narrowing factor of k as defined by Kauppinen et al. (*30*). For maximum likelihood restoration a Lorentzian profile with FWHH of γ', no smooth, 0.2% of uncertainty and 10 000 iterations were used.

(B) Curve Fitting Procedures. Curve fitting was carried out using the program CURVEFIT supplied by Spectrum Square Associates, Inc., which uses the Levenberg−Marquardt method to find the parameters that yield a minimum χ^2. The program does not allow negative values for any parameter; when a parameter hits this limit, it was fixed to zero. Iterations were performed until a minimum was found or the χ^2 changed less than 1 in 10^5 in one iteration (our criteria of convergence) to a maximum of 1000 iterations.

(C) Curve Fit of Deconvoluted Spectra. To obtain accurate results on curve fitting overlapped bands, the shape of the component bands should be well characterized. The deconvolution procedure introduces changes in the band shapes. For an infrared spectrum composed by n pure Lorentzian bands with FWHH of γ_i, deconvolution will give a sum of bands with the following shape: a residual Lorentzian character with FWHH of $\gamma_i' = (\gamma_i - \gamma')$ convoluted with the Fourier transform of a Bessel function of FWHH equal to γ'/k (*31*). As the Fourier transform of a Bessel function resembles a Gaussian band, the new bands can be closely described as Voigt functions (convolution of a Lorentzian band and a Gaussian band). Therefore, the Voigt function was used to curve fit the deconvoluted spectra (suitability of this approach is shown in a paper being prepared for publication). A Voigt function contains four parameters: area, position, Lorentzian width, and Gaussian width. During the curve fitting procedure the Gaussian width (γ_G) is fixed to $0.94\gamma'/k$, and the rest of parameters are set free. After convergence, the fit gives the area (A_i), position (v_i), and Lorentzian FWHH (γ_i') of bands in the deconvoluted spectrum. Since the fitting algorithm does not allow negative values for γ_i', when this parameter reaches zero for any band, it cannot be distinguished if the band has been properly Fourier self-deconvoluted ($\gamma_i = \gamma'$) or overdeconvoluted ($\gamma_i < \gamma'$); in that case, γ_G was allowed to be adjusted during the curve fitting but constrained to be equal or lower than $0.94\gamma'/k$. Usually less than 200 iterations were needed to fulfill our criteria of convergence. No baseline was introduced in the curve fit (if baseline correction was needed, an offset was previously subtracted before the iterations were started). The number of bands introduced in the fit was determined as those visually observable at the spectrum, as clearly resolved maxima, or well-defined shoulders. The number of bands was limited by the following restriction: the residual at the amide I should be similar in amplitude to the noise observed after deconvolution in a near zone free of bands (around 1800 cm^{-1}). If the residual is too low, overfitting was concluded; on the other hand, the need of an extra band was detected when systematic deviations in the residual, higher than the noise, were observed. Also, as in deconvolution the interferogram is cut at $0.95k/\gamma'$ cm (*13*, *30*), the nominal resolution in the deconvoluted spectra becomes $1.05\gamma'/k$ cm^{-1}, putting a final limit to the number of bands possibly resolved after deconvolution (*13*).

(D) Curve Fit of Original Spectra. Since deconvolution does not distort the area or position of a individual band but reduces the Lorentzian width (*32*), all of the parameters can be directly translated from the deconvoluted to the original spectra, except for the Lorentzian width, that should be calculated using the expression $\gamma_i = (\gamma_i' + \gamma')$. For overdeconvoluted bands, original widths can roughly be estimated as $\gamma_i = k\gamma_G$. The curve fit of original spectra was done between 1850 and 1480 cm^{-1}. Voigt functions were introduced, keeping fixed the position and the Lorentzian width previously determined from the curve fit to a deconvoluted spectrum. The Gaussian width was fixed to zero, and only the band heights and a zero slope baseline were set free. Under these conditions the fit becomes a linear one. After convergence, all of the parameters of bands above 1700

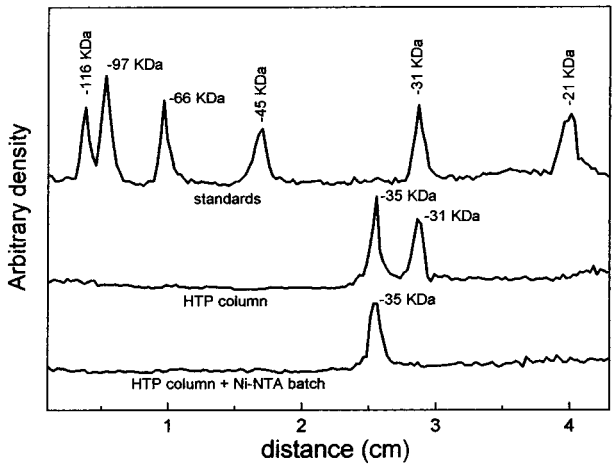

FIGURE 1: SDS−PAGE densitogram for the molecular mass standards (top), HTP column elution (middle), and HTP column elution further purified with a Ni−NTA resin (bottom). For the HTP and HTP + Ni−NTA lanes the molecular masses of the bands were obtained by interpolation from the standards. From band integration, the Ancp2His purity was estimated to be better than 95%.

cm^{-1} and below 1600 cm^{-1} (including the Gaussian width) were set free, and a minimum of 200 iterations were performed. Then, all of the parameters, except positions of bands between 1700 and 1600 cm^{-1}, were set free, and 1000 iterations were performed. Finally, all of the parameters were set free and 1000 iterations were performed.

RESULTS

As described in Materials and Methods, the carboxyatractyloside-inhibited Anc2pHis was purified from mitochondria in a two-step procedure: a hydroxylapatite (HTP) chromatography followed by affinity chromatography using a Ni−NTA resin. In Figure 1 the densitogram of different lanes obtained from a SDS−PAGE is displayed. The lane corresponding to the HTP column eluate shows only two bands: a 35 kDa band assigned to Ancp2His and a 31 kDa band assigned to the mitochondrial phosphate transporter (*20*). At this step of purification the Anc2pHis showed 60% purity. After the second step of purification (Ni−NTA batch), only one single band was evident, assigned to the Anc2pHis. The purity at this step was higher than 95% and thus was suitable for FTIR studies.

FTIR Characterization of Solubilized Anc2pHis. Figure 2A presents the spectrum of the carboxyatractyloside-inhibited Anc2pHis solubilized in DM, after buffer subtraction. A buffer subtraction factor of 0.971 was considered to be optimum, but factors from 0.975 to 0.967 gave also acceptable results. The amide I maximum was located at 1655.2 cm^{-1}, the amide II at 1546.7 cm^{-1}, and the tyrosine (from the fourth derivative) at 1517.1 cm^{-1}. The amide I/amide II ratio intensity was determined to be 1.44 ± 0.14, and the absorption coefficient was 192 ± 8 M^{-1} cm^{-1} for the amide II and 280 ± 40 M^{-1} cm^{-1} for the amide I, where the errors arise from the uncertainty in the factor of buffer subtraction. Figure 2A also shows the side chain amino acid absorption and the Anc2pHis spectrum once the amino acid side chain contribution was subtracted. To determine the scaling factor, protein concentration was taken as 10 mg/mL and the path length as 8.4 μm. It was calculated that 15.5% of the area

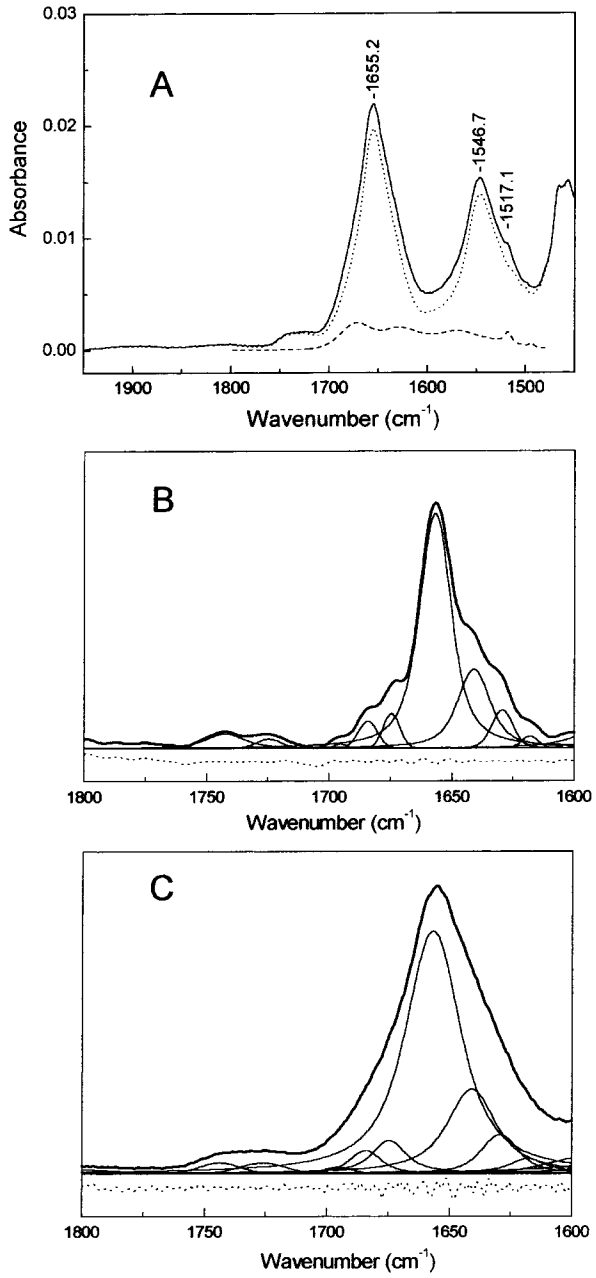

FIGURE 2: (A) (—) Transmission absorption spectrum of the solubilized carboxyatractyloside-inhibited Anc2pHis in H_2O at 25 °C once contributions arising from buffer have been subtracted. Before subtraction, the spectrum had a 0.88 AU in the amide I maximum (1655 cm^{-1}). The noise standard deviation (at 1825 cm^{-1}) was 2.2 × 10^{-5} AU. The noise standard deviation at the amide I maximum was calculated to be 1.4 × 10^{-4} AU, giving a S/N for the amide I equal to 150. (- - -) Synthetic amino acid side chain spectrum from the data reported by Venyaminov et al. (*24*). (•••) Anc2pHis spectrum once the amino acid contribution has been subtracted. (B) (—) Deconvolution and curve fit of the spectrum shown in (A) once the amino acid chain contribution (except that of tyrosine) has been removed. For the deconvolution the following parameters have been used: a Lorentzian band shape of $\gamma' = 18$ cm^{-1}, a $k = 2.0$, and a Bessel apodization, giving a new nominal resolution of 9.5 cm^{-1}. The results of the fit are presented in Table 1. (•••) Curve fit residual, at the same scale, shifted down for a clear display. (C) (—) Curve fit of the original spectrum shown in (A). The amino acid side chain contribution (except that of tyrosine) has been removed. The curve fit was performed as described in Materials and Methods, but the positions determined from the deconvoluted spectrum were fixed for bands assigned to amide I. Fit results are presented in Table 1. (•••) Curve fit residual multiplied by 5 and shifted down for a clear display.

Table 1: Summary of the Curve Fit to the Deconvoluted Spectrum of Solubilized Carboxyatractyloside-Inhibited Anc2pHis (Figure 2B) and the Curve Fit to the Original Spectrum Shown in Figure 2C, Together with the Proposed Assignments for the Bands

deconvoluted		original				
position[a]	% area	position[a]	FWHH[b]	% *L*[b]	% area	assignments
1742.4		1743.7	19	0		phospholipid C═O
1724.6		1726.2	22	0		phospholipid C═O
1695.3	0.4	1695.3	13	0	0.6	β-sheets
1684.2	3.5	1684.2	15	55	3.2	reverse turns
1674.6	4.0	1674.6	17	85	5.5	reverse turns
1656.6	64.2	1656.6	27	75	63.9	α-helix + unordered
1641.0	21.9	1641.0	24	85	20.2	β-sheets
1629.4	6.0	1629.4	18	55	6.5	β-sheets
1617.8		1617.8	16	100		tyrosine

[a] In cm^{-1}. [b] The Voigt function used to fit the original spectrum, described by the parameters Lorentzian width and Gaussian width, is presented as its equivalent mixed Gaussian−Lorentzian profile with two parameters: FWHH in cm^{-1} and the percentage in height of the Lorentzian character (% *L*).

from 1700 to 1480 cm^{-1} (baseline at 1850 cm^{-1}) corresponds to the side chain amino acid absorption. This is in good agreement with the value calculated following the procedure reported by Rahmelow et al. (*33*), which predicts a 16.7% from the primary sequence of Anc2pHis. When path length or protein concentration was unknown, data from Rahmelow et al. (*33*) were used to determine the subtraction factor for the amino acid side chain spectrum.

Secondary Structure Analysis: Curve Fit and Deconvolution. Figure 2B shows the deconvolution of the spectrum presented in Figure 2A (once the amino acid side chain contribution, except tyrosine, was subtracted). In the same figure the component bands obtained by curve fitting are also presented. Three bands were found to be overdeconvoluted as reported by the curve fit: 1695, 1675, and 1618 cm^{-1} bands. A curve fitting of the original spectrum was also performed (shown in Figure 2C). In this case, the data derived from the curve fit to the deconvoluted spectrum (number of bands, position, width) were used as the starting point of the curve fitting procedure. The fitting was carried out as described in Materials and Methods, but the last fitting step was omitted and band positions were kept fixed. This was done because the standard deviation of the residual was 7×10^{-5} AU, already lower than the noise standard deviation calculated at 1660−1630 cm^{-1} (1.5×10^{-4} AU), and therefore further reduction of the residual was meaningless.

Table 1 presents the parameters obtained from the curve fit to the deconvoluted as well as to the original spectra, together with the proposed assignments. The 1744 and 1726 cm^{-1} bands were assigned to the C═O stretching from the ester group of phospholipids. Using the integrated absorption coefficient of C═O phospholipid vibration (for egg PC) and the protein concentration, it was concluded than 15 ± 2 molecules of phospholipid kept bound per Anc2pHis dimer in the presence of DM. The 1618 cm^{-1} band was assigned to tyrosine. The rest of the bands were assigned according to reviewed data (*7, 34*).

The estimated secondary structure composition for the solubilized Anc2pHis−carboxyatractyloside complex in aqueous buffer (H_2O) averaged for two independent samples is presented in Table 4. The calculation was performed considering that the different secondary structures have different integrated absorption coefficients (*35*). This calculation was applied to the data derived from the curve fit to the deconvoluted spectrum and to the original spectrum; these estimations agreed within 4%. Different structure estimation could also be obtained from data in Table 1, assuming that the area is just directly proportional to the amount of the assigned structure. Obviously, it will lead to overestimation of β-sheets and underestimation of turns, compared to the determination using the coefficients of de Jong et al. (*35*). Which solution is more exact is a matter of debate, since the relative integrated absorption coefficient for turns with respect to β-sheets determined by de Jong et al. (*35*) is very imprecise (0.3 ± 0.2).

It can be concluded that the carboxyatractyloside-inhibited Anc2pHis in the solubilized state has mainly α-helix plus unordered structures (about 60%), compatible with the predicted 40% of the amino acids forming six transmembrane α-helices for the Anc2p (*36*). Later on, the problem of discriminating the α-helix and unordered contributions will be assessed for the reconstituted state.

Dry Film of Solubilized Anc2pHis. The interest in studying a dry film of a protein by FTIR comes mainly from the difficulties, when working with protein aqueous solutions (H_2O), to obtain an amide I profile with sufficient S/N for the analysis requirements. This low S/N in solution comes from the strong water absorption at 1645 cm^{-1}. Moreover, buffer subtraction, an unavoidable step prior to any analysis, is prone to errors and personal bias (*26*). In contrast, when proteins are studied in dry films, high S/N is commonly achieved, and water subtraction is not necessary for analysis. Artifacts may appear in this case, however, from protein structural changes upon dehydration, although several studies (*15, 37*) suggest that these effects are not common, even for soluble proteins.

Figure 3A shows a transmission absorption spectrum of a dry film of the solubilized carboxyatractyloside-inhibited Anc2pHis. Amide I maximum is shifted upward 2.3 cm^{-1} and the amide II maximum downward 0.7 cm^{-1} with respect to that of solution. These shifts are in agreement with differences generally observed between solution samples and film samples (*15*). The amide I/amide II intensity ratio was 1.68, suggesting that some water may be present in the dry film. This could not be directly checked at 3400 cm^{-1} as DM absorbs between 3500 and 3200 cm^{-1} (sugar O−H stretching). Taking into account the DM acyl integrated absorption coefficient and the DM-to-protein ratio (9:1 w/w), it was possible to determine the amount of protein (0.084 ± 0.004 mg cm^{-2}) and the peptide bond absorption coefficient for the amide I (370 ± 30 M^{-1} cm^{-1}) and the amide II (220 ± 20 M^{-1} cm^{-1}) bands. The amide II coefficient is in agreement with that of solution, but the amide I coefficient is significantly higher, indicating that remaining water is present in the film. The amino acid side chain absorption spectrum was subtracted with a factor derived from the calculated amount of protein.

Figure 3B shows the deconvoluted spectrum of Figure 3A. Since under the optimal conditions of deconvolution the spectrum appears less defined than the spectrum of the liquid sample, two different sets of deconvolution parameters were used; one (top trace) was used to determine the number of

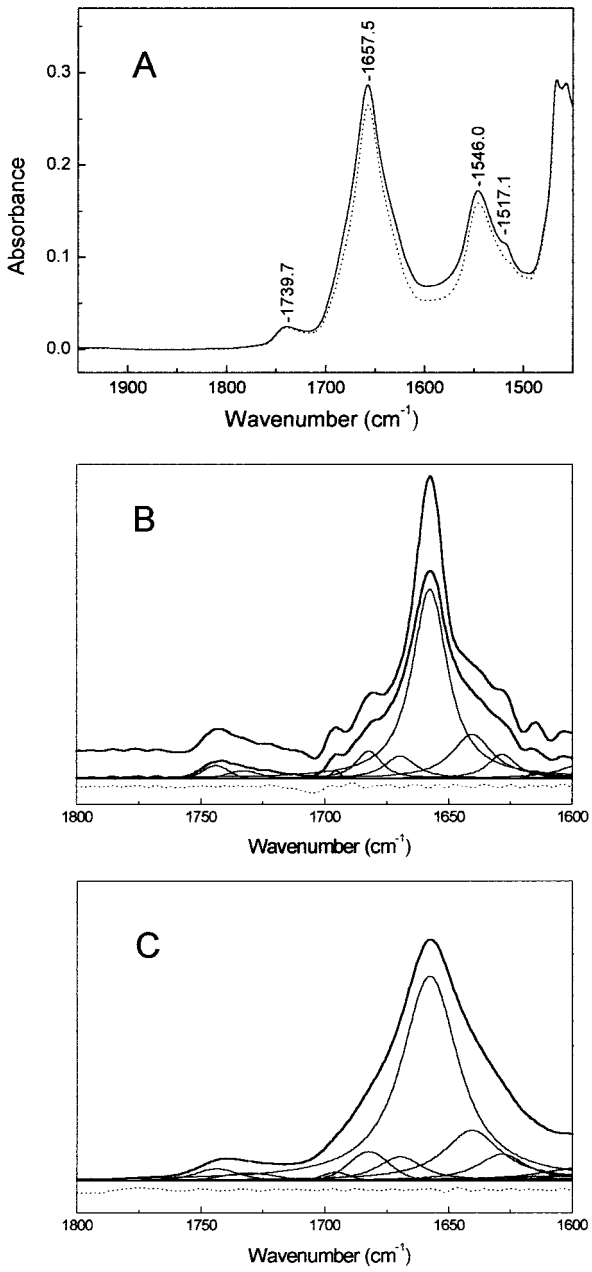

FIGURE 3: (A) (—) Transmission absorption spectrum of a dry film of the solubilized carboxyatractyloside-inhibited Anc2pHis at 25 °C. No buffer subtraction was performed. The noise standard deviation was 2×10^{-5} AU at 1850 cm^{-1}. At the amide I maximum (0.3 AU in the recorded spectrum) the calculated noise standard deviation was 4×10^{-5} AU, and the S/N was 7000. (···) Same spectrum after the synthetic amino acid side chain absorption spectrum was subtracted. (B) (—) Deconvolution of the spectra shown in (A) once the amino acid chain contribution, except that of tyrosine, has been removed. Top trace (shifted up for clarity): $\gamma' = 18$ cm^{-1}, $k = 2.5$, and Bessel apodization, giving a nominal resolution of 7.6 cm^{-1}. This spectrum was used to determine the number of bands. Down trace: $\gamma' = 12$ cm^{-1}, $k = 2.5$, and Bessel apodization, giving a nominal resolution of 5.0 cm^{-1}. This spectrum was curve fitted as described in Materials and Methods. The results of the fit are presented in Table 2. (···) Curve fit residual shifted down for a clearer display (at the same scale). (C) (—) Curve fit of the original spectrum shown in (A) once the amino acid side chain contribution (except that of tyrosine) has been removed. The fit was performed as described in Materials and Methods, giving as initial values the parameters from the spectra showed in (B). The results are presented in Table 2. (···) Curve fit residual multiplied by 20 and shifted down for a clearer display.

Table 2: Summary of the Curve Fit to the Deconvoluted Spectrum of a Dry Film of the Solubilized Carboxyatractyloside-Inhibited Anc2pHis (Figure 3B) and the Curve Fit to the Original Spectrum Shown in Figure 3C, Together with the Proposed Assignments for the Bands

deconvoluted		original				
position[a]	% area	position[a]	FWHH[b]	% L[b]	% area	assignment
1743.9		1743.7	19.1	40		phospholipid C═O
1732.8		1731.6	27.2	35		phospholipid C═O
1695.5	0.5	1696.1	12.2	10	0.8	β-sheets
1682.2	6.5	1682.5	19.7	10	5.2	reverse turns
1669.6	6.6	1669.6	20.5	75	5.3	reverse turns
1657.6	63.4	1657.7	27.1	95	64.6	α-helix + unordered
1640.5	16.7	1641.1	27.9	90	16.5	β-sheets
1628.4	6.3	1628.4	23.8	85	7.4	β-sheets
1614.8		1614.8	11.7	100		tyrosine

[a] In cm^{-1}. [b] The Voigt function used to fit the original spectrum, described by the parameters Lorentzian width and Gaussian width, is presented as its equivalent mixed Gaussian−Lorentzian profile with two parameters: FWHH in cm^{-1} and the percentage in height of the Lorentzian character (% L).

bands, while the other (down trace) was curve fitted. The best fitted bands are displayed in the same figure, and their parameters are presented in Table 2. Figure 3C presents the curve fit to the original spectrum, using as initial values those obtained from Figure 3B. Table 2 presents the results of the curve fit, together with the proposed assignments. The 1744 and 1732 cm^{-1} bands were assigned again to phospholipid. From the integrated absorption coefficient of the C═O group from egg PC, it was calculated that 18 ± 6 molecules of phospholipid remained bound per Anc2pHis dimer. The band at 1615 cm^{-1} was assigned to tyrosine following the results of Rahmelow et al. (*25*) and Chirgadze et al. (*33*). These authors reported an integrated absorption coefficient of 5×10^3 $mmol^{-1}$ cm^{-2}, whereas using the area of the curve fit in Figure 3C and taking into account 11 tyrosines per monomer, an integrated absorption coefficient of 6×10^3 $mmol^{-1}$ cm^{-2} was calculated. This good agreement for such a small band, although it is not fundamental in our study, shows the accuracy gained on working with dry film.

Table 4 collects the secondary structure estimation for the dry Anc2pHis film derived from curve fit of the deconvoluted spectra and curve fit of the original spectra. These data closely compare with the data from the sample in solution, presented in Table 4 as well. The estimation based on the original spectra agrees within 2−3%, whereas the estimation based on the deconvoluted spectra agrees within 3−8%. Furthermore, when individual bands are compared (Tables 1 and 2), the similitude is still remarkably good. It can be concluded that the structure of the carboxyatractyloside-inhibited Anc2pHis is well preserved in the film state. This is not surprising since some water always remains bound to the protein, even in a dry film. Moreover, DM has a sugar moiety, and sugars are often used to protect proteins against dryness (*38*).

Dry Film of the Reconstituted Anc2pHis. The good conservation of the secondary structure in the dry film of the solubilized Anc2pHis encouraged the extension of the work to dry films of the carrier reconstituted in phospholipids (egg PC/PA). The dry film of the reconstituted protein was

measured by FTIR-ATR spectroscopy, which facilitates sample preparation and H/D exchange experiments. However, FTIR-ATR can complicate the quantitative analysis of the spectra, since the spectra depend on film thickness (*15*) and sample orientation (*29*). First, we investigated if the film of the reconstituted Anc2pHis follows the thin or the thick film hypothesis. The ratio of the lipid C═O band (area over 1770−1710 cm^{-1}) to the acyl band (area over 3000−2800 cm^{-1}) obtained from the ATR spectrum was compared with a transmittance one. The resulting proportion, close to 1.0, indicates that the film follows the thin film hypothesis. Moreover, from the lipid-to-protein ratio and the integrated absorption coefficients of the egg PC acyl and carbonyl groups, the effective path length was calculated to be 0.5 μm for both bands. In contrast, the thick film hypothesis predicts a different path length for both bands (2.5 and 4.2 μm, respectively), supporting the conclusion that the sample is described by the thin film hypothesis.

Figure 4A shows the absorption spectrum of a dry film of the reconstituted carboxyatractyloside-inhibited Anc2pHis. This spectrum presents some differences with respect to that of Figure 3A, as the amide I and II maxima are shifted 1 cm^{-1} up and 0.3 cm^{-1} down, respectively, and the amide I/amide II intensity ratio is 1.81, higher than in the presence of detergent. These differences could be assigned to a different structure in the solubilized and reconstituted state, and/or a higher amount of residual water. It should be pointed out that an orientation effect, due to the alignment of the phospholipid bilayers parallel to the ATR crystal surface, with the roughly perpendicular orientation of the transmembrane α-helices, cannot explain the higher amide I/amide II intensity ratio for a thin film, as is the case (see Materials and Methods). Then, the contribution of remaining water to the spectrum was carefully examined. The amide A (3295 cm^{-1}) and remaining water (at 3550 cm^{-1}) can be observed without interferences. A wet film of egg PC was used to obtain the absorption from water molecules that remain bound in a film sample, concluding that the water band at 3400 cm^{-1} displayed the same width as in solution, and therefore the same absorption coefficient at the maximum can be expected (100 M^{-1} cm^{-1}). From this, an approximated absorption coefficient for water at 3550 cm^{-1} of 60 M^{-1} cm^{-1} was used. Taking $\epsilon_{amideI} = 370 \pm 30$ M^{-1} cm^{-1} and $\epsilon_{amideII} = 220 \pm 20$ M^{-1} cm^{-1}, 400−600 molecules of water were calculated to remain bound per Anc2pHis dimer (0.15 g of H_2O/g of Anc2pHis) in the dry film. This amount is enough to ensure hydration, even for many soluble proteins (*15*). The water band at 1645 cm^{-1} was estimated to have a height of only 0.006 AU (5% of amide I maximum) with an 80 cm^{-1} FWHH. After this correction the amide I/amide II intensity ratio became 1.73, suggesting structure differences with respect to the solubilized form.

Lipid−Protein Interactions in the Reconstituted Protein. Several spectroscopic tests were carried out to determine whether the reconstitution was successfully performed. The starting reconstitution mixture was prepared at a lipid-to-protein ratio (w/w) of 3.0. From the lipid C═O band area and the amide I and amide II height, it was determined that the lipid-to-protein ratio was between 3.0 and 2.5 (300−240 phospholipids per Anc2pHis dimer) so no significant amount of protein was lost during the purification, as this would give rise to an increase of the lipid-to-protein ratio.

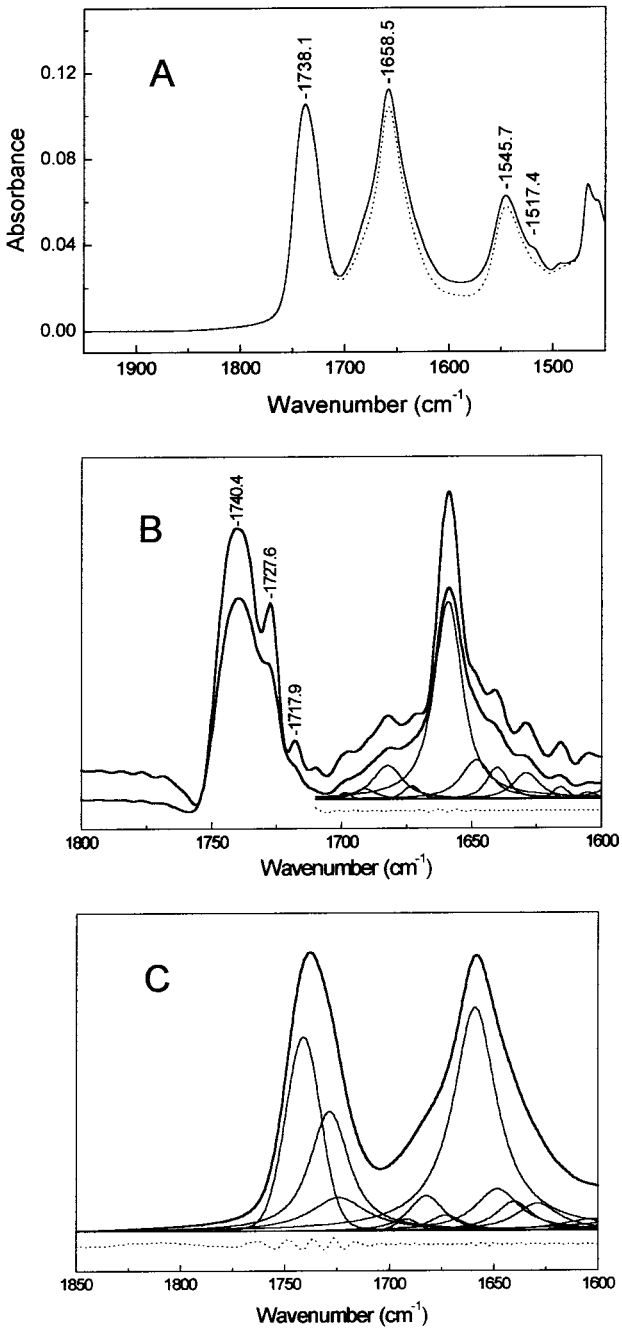

FIGURE 4: (A) (—) ATR spectrum of a dry film at 26 °C of the carboxyatractyloside-inhibited Anc2pHis reconstituted in egg PC/PA. The S/N at the amide I band maximum was 17 000. (···) Same spectrum after the synthetic amino acid side chain absorption spectra was subtracted. (B) (—) Deconvolution and curve fit of the spectra shown in (A) once the amino acid side chain contribution (except that of tyrosine) has been removed. Top trace (shifted for clarity): $\gamma' = 18$ cm^{-1}, $k = 3.0$, and Bessel apodization, giving a nominal resolution of 6.3 cm^{-1}. This spectrum was used to determine the number of bands. Down trace: $\gamma' = 14$ cm^{-1}, $k = 2.5$, and Bessel apodization, giving a nominal resolution of 5.9 cm^{-1}. This spectrum was curve fitted as described in Materials and Methods. The results of the fit are presented in Table 3. (···) Curve fit residual shifted down for clarity (at the same scale). (C) (—) Curve fit of the spectrum shown in Figure 3A once the amino acid side chain contribution (except that of tyrosine) has been removed. The fit was performed giving as initial values parameters derived from (B). Fit results are presented in Table 3. (···) Curve fit residual multiplied by 10 and shifted down for a clearer display.

We can also conclude that the protein−lipid mixture was preserved in the film attached to the ATR germanium surface.

To know if the protein was interacting with the lipids, we studied how the presence of the protein affects the phospholipid IR bands. Two phospholipid regions were investigated: the phospholipid antisymmetric and symmetric CH_2 stretching, which are sensitive to the gel-to-liquid crystal phase transition of the lipid, and the C═O stretching, sensitive to the hydrogen bonding and thus to the hydration state. Pure egg PC/PA in aqueous suspension is (at room temperature) in the liquid crystal phase, but it shifts to the gel phase when dried (gel-to-liquid transition in dry films occurs around 42 °C). We observed that, although the sample was dry, the CH_2 stretching bands corresponding to the sample in Figure 4A appear at 2923.4 and 2853.2 cm^{-1}, which are similar to those found for pure egg PC/PA in solution at room temperature: 2923.3 and 2853.1 cm^{-1} (spectra not shown). This can be explained considering that the interaction with the protein is driving the phospholipid to the liquid crystal phase, even in a dry film at room temperature. On the other hand, the phospholipid C═O stretching appears at 1738.1 cm^{-1}, similar to the value found for pure egg PC/PA in the dry state. However, deconvolution of this band (see Figure 4B) reveals at least three components, at 1740.4, 1727.6, and 1717.9 cm^{-1}. When deconvolution with the same parameters was applied to a dry film of pure egg PC/PA, only one band (1738.9 cm^{-1}) and a shoulder ($\approx$1730 cm^{-1}) were apparent, while a wet film gave two broad bands (1741.9 and 1730.2 cm^{-1}) (not shown). It can be concluded than the 1727.6 and 1717.9 cm^{-1} bands appearing in the reconstituted Anc2pHis film came from hydrogen bonding of the lipid C═O, probably to amino acid side chain residues of the protein, since some of these interactions (those giving rise to the 1717.9 cm^{-1} band) were very strong.

Secondary Structure Analysis of Dry Reconstituted Film: Curve Fit and Deconvolution. Figure 4B shows the results of the deconvolution of the spectrum in Figure 4A using two different sets of deconvolution parameters; the top trace was used to determine the number of bands, and the down trace was curve fitted (fitted bands are also presented). Figure 4C shows the curve fitting of the original spectrum. The results of both curve fittings are presented in Table 3, whereas the secondary structure estimation is presented in Table 4. Two effects could reduce the quality of secondary structure estimation: the remaining water and sample orientation. The effect of the remaining water in the curve fit results was analyzed for the deconvoluted spectrum shown in Figure 4B (down trace) by introducing in the fit a synthetic band representing the water contribution with all parameters fixed (see above). Only minor differences were observed when area results are compared band to band to those in Table 3. The secondary structure estimation changes to the following: reverse turns = 26.2%; β-sheets = 8.6%; α-helix + unordered = 65.2% (see Table 4 for a comparison). With respect to the orientation effect on the secondary structure estimation, only transmembrane α-helices are prone to be significantly oriented in dry film. From the literature, the order parameter for the amide I dipole transition moment of transmembrane α-helices of proteins with respect to the crystal surface normal usually obtained for an oriented sample ranges from $p = 0.35$ to $p = 0.2$ (*34*, *39*−*42*). If this orientation is accepted for the transmembrane helices of Anc2p, considering that they are predicted to account for 40% of the secondary structure, the results presented in Table 4 for the secondary structure estimation from the original spectrum should change to the following: reverse turns = 21%; β-sheets = 8.5%; α-helix + unordered = 70.5%; that means only slight differences.

Table 3: Summary of the Curve Fit to the Deconvoluted Spectrum of a Dry Film of the Reconstituted Carboxyatractyloside-Inhibited Anc2pHis (Figure 4B) and the Curve Fit to the Original Spectrum Shown in Figure 4C, Together with the Proposed Assignments for the Bands

deconvoluted		original				
position[a]	% area	position[a]	FWHH[b]	% *L*[b]	% area	assignments
1698.5	0.6	1699.4	9.8	0	0.4	β-sheet
1691.0	2.4	1691.7	12.9	0	1.2	reverse turns
1682.2	10.3	1682.3	19.5	80	7.2	reverse turns
1673.0	2.1	1673.1	19.0	100	3.3	reverse turns
1659.0	58.6	1659.1	25.2	100	61.7	α-helix + unordered
1648.1	12.3	1648.3	25.7	100	11.8	α-helix + unordered
1640.1	6.8	1640.3	21.1	100	6.8	β-sheets
1628.9	7.0	1629.1	25.0	100	7.6	β-sheets
1615.8		1616.1	12.3	90		tyrosine

[a] In cm^{-1}. [b] The Voigt function used to fit the original spectrum, described by the parameters Lorentzian width and Gaussian width, is presented as its equivalent mixed Gaussian−Lorentzian profile with two parameters: FWHH in cm^{-1} and the percentage in height of the Lorentzian character (% *L*).

Table 4: Estimated Secondary Structure Composition for the Carboxyatractyloside-Inhibited Anc2pHis in Three Different Physical States: Solubilized, Solubilized in Dry Film, and Reconstituted in Dry Film

	solubilized (%)[a]		solubilized (dry) (%)		reconstituted (dry) (%)	
secondary structure[b]	deconvoluted	original	deconvoluted	original	deconvoluted	original
reverse turns	17 ± 2	18.7 ± 1.3	25.6	21.4	27.7	22.6
β-sheets	18 ± 4	19.7 ± 0.6	15.2	16.4	8.9	9.5
α-helix + unordered	65 ± 2	61.6 ± 0.7	59.2	62.2	63.4	67.9

[a] For the solubilized form the data refer to two independent samples with its standard deviation. [b] It was considered that the different structures have different integrated absorption coefficients in the amide I region, following the relation reported by de Jong et al. (*35*) (β:α:turns 1:0.69:0.33), where unordered structures were included with α-helix structures. Results are presented from two data sources: deconvoluted and original spectrum (see Tables 1−3).

Two important changes are visible in the dry film of the reconstituted carboxyatractyloside-inhibited Anc2pHis, compared to the dry film of the solubilized protein: a shift of the main band from 1657.7 cm^{-1} in the solubilized to 1659.1 cm^{-1} in the reconstituted form and a new band at 1648 cm^{-1}, with the 1640 cm^{-1} band reducing significantly its area and its width. The secondary structure estimation (Table 4) also reflects these differences, with reduction of β-sheet structures and increase of α-helix and/or unordered structures. The reconstituted spectrum showed a much higher S/N, allowing a higher narrowing factor (and final nominal resolution) than that used for the solubilized sample ($k = 3$ vs $k = 2.5$). These differences in the deconvolution parameters might be the reason for resolving a new band at 1648 cm^{-1}. When applying to the reconstituted sample the narrowing factor

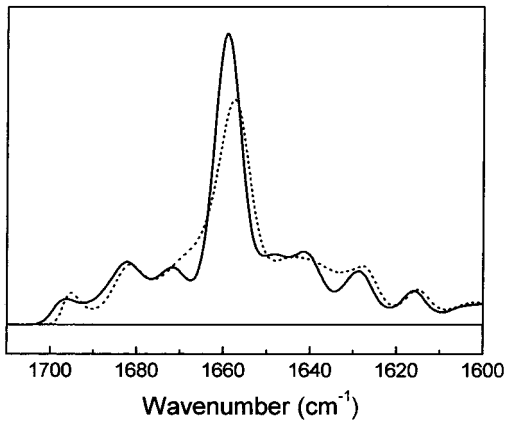

FIGURE 5: Amide I of the carboxyatractyloside-inhibited Anc2pHis in (···) dry solubilized form and (—) dry reconstituted form, after nonlinear deconvolution using a maximum likelihood algorithm with $\gamma' = 20$ cm^{-1} (Lorentzian). Both spectral areas were normalized between 1710 and 1600 cm^{-1}.

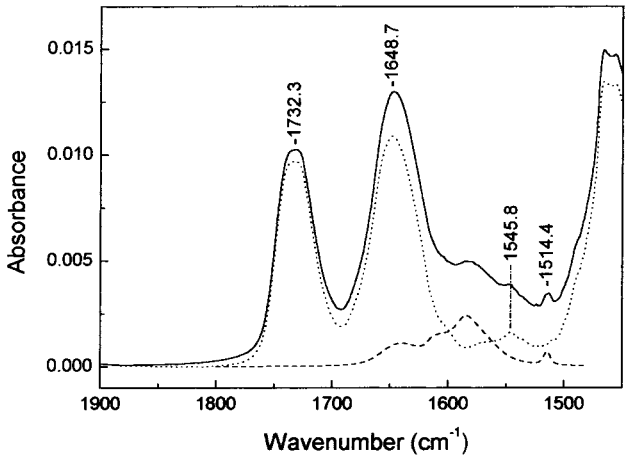

FIGURE 6: (—) ATR spectrum of a wet film of reconstituted carboxyatractyloside-inhibited Anc2pHis after 15 h of H/D exchange. The S/N at the amide I maximum was 2200. (···) Same spectrum after the amino acid side chain spectrum and the D_2O contribution were subtracted. (- - -) Synthetic deuterated amino acid side chain absorption calculated from the data reported by Chirgadze et al. (*25*).

originally used with the solubilized one, the 1648 cm^{-1} band was not completely resolved, appearing only as a faint shoulder. To solve this problem, both spectra were deconvoluted with a nonlinear deconvolution algorithm (maximum likelihood restoration) in which the differences in S/N are not as critical as in Fourier self-deconvolution and identical parameters for both spectra could be used. Both deconvoluted spectra are presented in Figure 5, where it can be confirmed that the appearance of a new band at 1648 cm^{-1} is not a noise-induced difference, thus confirming the structural differences between reconstituted and solubilized samples.

Hydrogen−Deuterium Exchange of Reconstituted Anc2pHis in Wet Film. Figure 6 shows the ATR spectrum of a wet film of the reconstituted carboxyatractyloside-inhibited Anc2pHis after 15 h of H/D exchange. The water concentration in the D_2O wet film and the path length can be calculated from the 2500 cm^{-1} D_2O band ($\epsilon_{2500} = 74.5$ M^{-1} cm^{-1}) and the C═O lipid band (see above). The effective path length was 1.2 μm at 1740 cm^{-1}, water concentration 40 M, and Anc2pHis concentration in the film around 80 mg/mL. These values show that the film is well hydrated.

Table 5: Summary of the Curve Fit to the Deconvoluted Spectrum and to the Original Spectrum of the Deuterated Reconstituted Carboxyatractyloside-Inhibited Anc2pHis Shown in Figure 6

deconvoluted		original		
position[a]	% area	position[a]	% area	assignments[b]
1680.0	1.6	1679.9	2.9	2.5% D-reverse turns + 0.4% D-β-sheets
1669.0	8.4	1668.6	7.3	7.3% D-reverse turns
1659.2	13.5	1659.1	13.7	11.8% H-α-helix + 1.9% D-reverse turns
1650.3	30.3	1650.3	30.9	30.9% D-α-helix (from 1659)
1640.7	21.2	1640.7	20.7	19% D-unordered (from 1659) + 1.7% H-β-sheets
1632.5	17.3	1632.5	17.4	11.8% D-unordered (from 1648) + 5.6% D-β-sheets
1623.4	7.7	1623.3	7.1	7.1% D-β-sheets
1612.5		1612.7		tyrosine

[a] In cm^{-1}. [b] The D prefix refers to a deuterated structure and the H prefix to a hydrogenated one (nonexchanged). For more information about how the assignments were performed, see the text.

In the exchanged spectrum the amide I′ maximum was shifted 10 cm^{-1} down, and the amide II intensity was strongly reduced, showing extensive exchange of the amide hydrogen atoms. The synthetic deuterated amino acid side chain spectrum was subtracted, being the scaling factor that needed to eliminate the tyrosine band (highly resolved in the deuterated form). After this operation the residual amide II became apparent. The maximum of residual II (1546 cm^{-1}) suggests that nonexchanged amide hydrogens are in α-helix structures. The percentage of nonexchanged amide hydrogens was determined from the relation between the amide II to amide I area ratio after and before deuteration, once the amino acid side chain contribution was subtracted. Notice that as both amide II and amide I bands come from the same chemical group and are close together in the spectrum, the amide II to amide I ratio corrects itself for any swelling of the film (*15*). It was determined (testing two different integration intervals for the amide II) that 13−20% of the amide hydrogens remained not exchanged after 15 h in the presence of D_2O vapor. We want to stress that amino acid side chain absorption was previously subtracted before the level of exchange was determined; otherwise, nonsense results would be obtained, since the area integrated under the amide II interval would gave negative values, leading to apparently more that 100% exchange.

The amide I of this corrected spectrum was analyzed by deconvolution and curve fit, as those spectra of Figure 3A and 4A (not shown). First, bands were identified in a spectrum deconvolved with $\gamma' = 18$ cm^{-1} and $k = 2.6$, and these bands where fitted in a spectrum deconvolved with $\gamma' = 14$ cm^{-1} and $k = 2.2$. The obtained results about number, position, and width of bands were used as initial values for a curve fit in the original amide I. Table 5 shows the curve fit results. The assignments were done following four premises: when completely deuterated, amide I bands should be shifted down about 5 cm^{-1} for β-sheets (*10*), about 10 cm^{-1} for α-helices (*10*), and between 15 and 20 cm^{-1} for unordered structures (*7*); the secondary structure assignments must show coherence to those in H_2O; about 15% of the amide I area should not be shifted (as is not exchanged) being this area mainly in α-helix bands; and unordered structures and reverse turns should be completely exchanged.

The assignments in Table 5 fulfill the criteria we imposed: the areas assigned to α-helix + unordered, to β-sheets, and to reverse turn structures are the same as in H_2O; the area assigned to nonexchanged structures represents 14% of the amide I area; 90% of the nonexchanged structures belongs to α-helix; and the exchanged α-helix shifted about 9 cm^{-1}, the exchanged β-sheets shifted 7.5−5.5 cm^{-1}, and unordered structures shifted between 18.5 and 15.5 cm^{-1}. Reverse turns showed an exchange-induced shift between 14 and 11 cm^{-1}. Table 5 assignments allow discriminating between α-helix and unordered contributions; thus the amide I area assigned to the different secondary structures becomes 44.4% α-helix, 29.1% unordered, 14.8% β-sheets, and 11.7% reverse turns. When the extinction coefficients proposed for the different secondary structures are used (*35*), the secondary structure estimation becomes 33.1% α-helix, 39.3% unordered, 7.6% β-sheets, and 20.0% reverse turns. The α-helix percentage is in this case lower than expected for the proposed 6 spanning membrane α-helices. A 44.4% percentage is consistent with up to 6.5 spanning membrane α-helices, but 33.1% is consistent with a maximum of 5 spanning membrane α-helices. This last value could be increased if an orientation of the transmembrane α-helix similar to that described in the literature was considered, to a final percentage ranging between 40% and 36%, and thus approaching the proposed 6 spanning membrane α-helices.

The structure assignment done with the D_2O-exchanged film allows discriminating between both bands assigned to α-helix + unordered structures in Table 3. Thus, most likely the 1648 cm^{-1} band comes completely from unordered structures and the 1659 cm^{-1} comes mainly from α-helix, although with an important unordered contribution.

DISCUSSION

We present in this paper an infrared spectroscopy study of the carboxyatractyloside-inhibited mitochondrial ADP/ATP transporter purified from the yeast *S. cerevisiae*. The carboxyatractyloside is noncovalently bound to the transporter with very high affinity, blocking it into a defined and probably functionally important conformation of the transporting cycle (*1*). Indirect evidence of an actual binding of the inhibitor to the protein was obtained from intrinsic fluorescence and FTIR studies (data not shown). When the solubilized inhibited form was heated, an intrinsic fluorescence transition was observed in which the fluorescence strongly increased. Because binding of the inhibitor to the solubilized protein decreases the intrinsic fluorescence (*17*), we interpreted that the fluorescence transition is caused by the release of the inhibitor from the protein. More importantly, this transition was not present when the Anc2pHis was isolated in the absence of inhibitor. Moreover, the free protein showed in the FTIR spectra very intense aggregation bands, not evident in the inhibited form.

The carboxyatractyloside-inhibited Anc2pHis has been studied in three states: solubilized in solution and in dry film and reconstituted in dry film. For all of these states, a minimum of 60% and a maximum of 70% of the protein are predicted to be in a helix conformation and/or adopting unordered structures. This percentage is consistent with the predicted six transmembrane helices that would account for 40% of the secondary structure (*36*) and allow between one-third and one-half of the topological loops to adopt helix and/or unordered structures. For the reconstituted protein, spectra deconvolution after H/D exchange experiments allows discriminating between α-helix and unordered structures. Thus, it can be concluded that the band at 1659 cm^{-1} accounts for 5−6.5 transmembrane helices. Although this result does not indicate exactly the number of helices, it is in keeping with the predicted six transmembrane helices.

Starting from the solubilized state (studied by transmittance), we found very small changes in the amount of secondary components on drying the protein. Moreover, the individual bands determined by deconvolution showed only small differences. This suggested to us to work with dry films for the reconstituted sample. The possible sources of errors on working with films, such as changes of structure upon dehydration, remaining water contribution to the amide I, and sample orientation, were carefully analyzed. It can be concluded that these errors do not significantly alter the secondary structure estimation. The preservation of the essential secondary structure of the Anc2p carrier in dry films is an important observation. This finding supports the extension of the structural studies to film preparations and controlled dry systems to investigate more subtle interactions, like H/D exchange, substrate binding, or the role of lipid environment.

When the amide I band for the reconstituted and the solubilized carboxyatractyloside-inhibited Anc2pHis is compared, some differences can be observed: first, some changes in the bands assigned to turns, second, the main band appears at different positions (1659.1 and 1657.7 cm^{-1}, respectively), and third, the main difference is the appearance of one band at 1648 cm^{-1}, with the concomitant decrease of the band at 1640 cm^{-1}. Using a nonlinear deconvolution algorithm to confirm these observations, we were able to discard any fictitious origin of these changes that could be due to differences in the parameters used in deconvolution. Assigning the 1648 cm^{-1} band to unordered structures, then the structural differences caused by the change from a detergent to a lipid environment are a decrease of β-sheets with an increase of unordered structures. This change involves 6−10% of the amino acids (20−30 residues). It can be concluded that the presence of phospholipids around the Anc2p polypeptide modulates the secondary conformation of the carrier, at least as compared with the conformation found in the detergent-solubilized form. Moreover, the lipid-induced changes were accompanied by protein-induced changes into the lipid environment. On one hand, the lipids present in the dry film of reconstituted Anc2pHis were in the gel state, whereas those of a dry film of pure egg PC/PA mixture were in the liquid crystal state. Additionally, the lipids in the reconstituted sample showed a stronger hydrogen bonding in the C═O groups, probably to some residues of the protein. These findings indicate that, after reconstitution and film preparation, an extensive contact between the transporter and the lipid molecules is achieved. Moreover, it can be suggested that the phospholipid environment has some role in the maintenance of the native conformation of the carrier in the mitochondrial membrane.

Hydrogen/deuterium exchange experiments were carried out in the reconstituted carboxyatractyloside-inhibited Anc2pHis. Most of the amide hydrogens were exchanged in 15 h (85%), and the remaining (about 50 amino acids)

were in α-helix structures, probably in transmembrane helices. This high percentage of exchange is roughly similar to the observed exchange of other α-helical transmembrane carriers of hydrophilic substrates such as the glucose erythrocyte carrier (85%) (*43*), the lactose permease from *E. coli* (100%) (*44*), or the melibiose permease from *E. coli* (80%) (*45*). These values are in clear contrast with those reported for aqueous channels as the *β*-structured porin from *E. coli* (35%) (*46*), the transmembrane α-helix aquaporin-1 from human erythrocyte (40%) (*47*), and the aerolysin from *Aeromonas hydrophila* (30%) (*48*), and for the transmembrane α-helix retinal proteins, which show less than 33% exchange (*47*, *49*). However, it should be mentioned that for the Anc2pHis the percentage of exchange has been calculated after correction for a full exchange of side chain protons, and many of the cited papers did not do so. For the Anc2pHis, this correction reduced the apparent observed exchange from about 100% to 85% and should be taken into account when comparing the degree of accessibility of different proteins. Assuming that the six transmembrane helical model is correct, the 85% exchange means that, in the carboxyatractyloside-inhibited form of Anc2p, not only the loops going out of the membrane but most of transmembrane helix peptide bonds (about 60% of them) are exchanged. This result implies that, even in that functionally blocked conformation of the carrier, most of the transmembrane helices are readily accessible to water molecules and show enough conformational flexibility to allow the observed amount of exchange.

Finally, it should be noted that, to carry out the secondary structure estimation, we introduced for the first time to our knowledge the use of Voigt bands to fit the deconvoluted spectra. This provides a close approximation to any band shape distortion caused by deconvolution. Tests made with synthetic amide I composed of pure Lorentzian bands showed the suitability of this approach to recover close estimations of area, position, and original width of the underlying bands (to be published). For synthetic amide I composed of bands with Lorentzian−Gaussian character, good results were obtained by performing a final fit to the original spectrum, starting from the parameters obtained by fitting a deconvolved spectrum.

REFERENCES

1. Fiore, C., Trézéguet, V., Le Saux, A., Roux, P., Schwimmer, C., Dianoux, A. C., Noël, F., Lauquin, G. J.-M., Brandolin, G., and Vignais, P. V. (1998) *Biochimie 80*, 137−150.
2. Adrian, G. S., McCammon, M. T., Montgomery, D. L., and Douglas, M. G. (1986) *Mol. Cell. Biol. 6*, 626−634.
3. Lawson, J. E., and Douglas, M. G. (1988) *J. Biol. Chem. 263*, 14812−14818.
4. Kolarov, J., Kolarova, N., and Nelson, N. (1990) *J. Biol. Chem. 265*, 12711−12716.
5. O'Malley, K., Pratt, P., Robertson, J., Lilly, M., and Douglas, M. G. (1982) *J. Biol. Chem. 257*, 2097−2103.
6. Drgon, T., Sabova, L., Nelson, N., and Kolarov, J. (1991) *FEBS Lett. 289*, 159−162.
7. Arrondo, J. L., Muga, A., Castresana, J., and Goñi, F. M. (1993) *Prog. Biophys. Mol. Biol. 59*, 23−56.
8. Goormaghtigh, E., Cabiaux, V., and Ruysschaert, J. M. (1994) *Subcell. Biochem. 23*, 329−362.
9. Goormaghtigh, E., Cabiaux, V., and Ruysschaert, J. M. (1994) *Subcell. Biochem. 23*, 405−450.
10. Krimm, S., and Bandekar, J. (1986) *Adv. Protein Chem. 3*, 181−364.
11. Venyaminov, S. Y., and Kalnin, N. N. (1990) *Biopolymers 30*, 1259−1271.
12. Bandekar, J. (1992) *Biochim. Biophys. Acta 1120*, 123−143.
13. Kauppinen, J. K., Moffatt, D. J., Mantsch, H. H., and Cameron, D. G. (1981) *Appl. Spectrosc. 35*, 271−276.
14. Byler, D. M., and Susi, H. (1986) *Biopolymers 25*, 469−487.
15. Goormaghtigh, E., Raussens, V., and Ruysschaert, J. M. (1999) *Biochim. Biophys. Acta 1422*, 105−185.
16. Klingenberg, M., Winkler, E., and Huang, S. (1995) *Methods Enzymol. 260*, 369−389.
17. Brandolin, G., Le Saux, A., Trézéguet, V., Vignais, P. V., and Lauquin, G. J.-M. (1993) *Biochem. Biophys. Res. Commun. 192*, 143−150.
18. Le Saux, A., Roux, P., Trézéguet, V., Fiore, C., Schwimmer, C., Dianoux, A.-C., Vignais, P.-V., Brandolin, G., and Lauquin, G.-J.-M. (1996) *Biochemistry 35*, 16116−16124.
19. Heidkämper, D., Müller, V., Nelson, D. R., and Klingenberg, M. (1996) *Biochemistry 35*, 16144−16152.
20. Fiore, C., Trézéguet, V., Roux, P., Le Saux, A., Noël, F., Schwimmer, C., Arlot, D., Dianoux, A.-C., Lauquin, G. J.-M., and Brandolin, G. (2000) *Protein Expression Purif. 19*, 57−65.
21. Daum, G., Bohni, P. C., and Schatz, G. (1982) *J. Biol. Chem. 257*, 13028−13033.
22. Krämer, R., and Klingenberg, M. (1979) *Biochemistry 18*, 4209−4215.
23. Smith, P. K., Krohn, R. I., Hermanson, G. T., Mallia, A. K., Gartner, F. H., Provenzano, M. D., Fujimoto, E. K., Goake, N. M., Olson, B. J., and Klenk, D. C. (1985) *Anal. Biochem. 150*, 76−85.
24. Venyaminov, S. Y., and Kalnin, N. N. (1990) *Biopolymers 30*, 1243−1257.
25. Chirgadze, Y. N., Fedorov, O. V., and Trushina, N. P. (1975) *Biopolymers 14*, 679−694.
26. Rahmelow, K., and Hübner, W. (1997) *Appl. Spectrosc. 51*, 160−170.
27. Carter, R. O., III, Lindsay, N. E., and Beduhn, D. (1990) *Appl. Spectrosc. 44*, 1147−1151.
28. Venyaminov, S. Y., and Prendergast, F. G. (1997) *Anal. Biochem. 248*, 234−245.
29. March, D. (1999) *Biophys. J. 77*, 2630−2637.
30. Kauppinen, J. K., Moffatt, D. J., Mantsch, H. H., and Cameron, D. G. (1981) *Anal. Chem. 53*, 1545−1457.
31. Griffihs, P. R., Pierce, J. A., and Hongin, G. (1987) in *Computer-Enhanced Analytical Spectroscopy* (Meuzelaar, H. L. C., and Isenhovic, T. L., Eds.) pp 29−54, Plenum Press, New York.
32. Cameron, D. G., and Moffat, D. J. (1984) *J. Test. Eval. 12*, 78−85.
33. Rahmelow, K., Hübner, W., and Ackermann, T. (1998) *Anal. Biochem. 257*, 1−11.
34. Tamm, L. K., and Tatulian, S. A. (1997) *Q. Rev. Biophys. 30*, 365−429.
35. de Jongh, H. H. J., Goormaghtigh, E., and Ruysschaert, J. M. (1996) *Anal. Biochem. 242*, 95−103.
36. Müller, V., Basset, G., Nelson, D. R., and Klingenberg, M. (1996) *Biochemistry 35*, 16132−16143.
37. Forato, L. A., Bernardes-Filho, R., and Colnago, L. A. (1998) *Anal. Biochem. 259*, 136−141.
38. Carpenter, J. F., and Crowe, J. H. (1989) *Biochemistry 28*, 3916−3922.
39. Earnest, T. N., Herzfeld, J., and Rothschild, K. J. (1990) *Biophys. J. 58*, 1539−1546.
40. Nabedryk, E., Tiede, D. M., Dutton, P. L., and Breton, J. (1982) *Biochim. Biophys. Acta 682*, 273−280.
41. Bazzi, M., and Woody, R. W. (1985) *Biophys. J. 48*, 957−966.
42. LeCoutre, J., Narasimhan, L. R., Patel, H. R., and Kaback, H. R. (1997) *Proc. Natl. Acad. Sci. U.S.A. 94*, 10167−10171.
43. Alvarez, J., Lee, D. C., Baldwin, D., and Chapman, D. (1987) *J. Biol. Chem. 262*, 3502−3509.
44. Patzlaff, J. S., Moeller, J. A., Barry, B. A., and Brooker, R. J. (1998) *Biochemistry 37*, 15363−15375.

45. Dave, N., Troullier, A., Mus-Veteau, I., Duñach, M., Leblanc, G., and Padrós, E. (2000) *Biophys. J. 79*, 747−755.
46. Kleffel, B., Garavito, R. M., Baumeinster, W., and Rosenbusch, J. P. (1985) *EMBO J. 4*, 1589−1592.
47. Cabiaux, V., Oberg, K. A., Pancoska, P., Walz, T., Agre, P., and Engel, A. (1997) *Biophys. J. 73*, 406−417.
48. Cabiaux, V., Buckley, J. T., Wattiez, R., Ruysschaert, J.-M., Parker, M. W., and van der Goot, F. (1997) *Biochemistry 36*, 15224−15232.
49. Rath, P., DeGrip, W. J., and Rothschild, K. J. (1998) *Biophys. J. 74*, 192−198.

BI010091S